Available online at www.sciencedirect.com
SCIENCE DIRECT®
Journal of Catalysis 220 (2003) 254–257
JOURNAL OF CATALYSIS
www.elsevier.com/locate/jcat

Research Note

Selective hydrogenation of 2-ethylanthraquinone over an environmentally benign Ni–B/SBA-15 catalyst prepared by a novel reductant–impregnation method

Xueying Chen, Huarong Hu, Bo Liu, Minghua Qiao,* Kangnian Fan, and Heyong He *

Laboratory of Molecular Catalysis and Innovative Materials, Department of Chemistry, Fudan University, Shanghai 200433, People's Republic of China

Received 8 May 2003; revised 27 June 2003; accepted 30 July 2003

Abstract

An environmentally benign SBA-15-supported amorphous nickel boride alloy catalyst, prepared by a novel reductant–impregnation method, exhibits superior activity, selectivity, and stability in the selective hydrogenation of 2-ethylanthraquinone (eAQ) to 2-ethylanthrahydroquinone (H_2eAQ), which is the dominating process for the production of hydrogen peroxide in industrial scale. The unique characters of the amorphous alloy as well as the pore structure of the mesoporous SBA-15 molecular sieve are crucial for the excellent catalytic behavior of the title catalyst.

Keywords: Ni–B; Mesoporous molecular sieve; SBA-15; eAQ; Hydrogenation; H_2O_2

1. Introduction

The hydrogenation of 2-ethylanthraquinone (eAQ) into 2-ethylanthrahydroquinone (H_2eAQ) is one of the key steps in the industrial manufacturing of H_2O_2, which is a non-polluting oxidizing agent [1–3]. In industry, Raney Ni and palladium are the most frequently used catalysts for this reaction. However, even on the most selective palladium catalyst some degradation products [3] are easily formed, which leads to the loss of fed hydrogen and the expensive eAQ. Moreover, the palladium catalyst is expensive. Thus, it is highly desirable to develop nonnoble catalysts with exclusive selectivity in carbonyl group hydrogenation, at the same time preventing hydrogenation of the aromatic ring.

In previous work, our group reported on two kinds of catalysts which exhibit higher selectivity than the conventional Raney Ni catalyst, one is the rapid-quenched skeletal Ni catalyst (RQ-Ni) and the other is a nanosized amorphous Ni–Cr–B catalyst [4,5]. However, a detailed chromatographic analysis reveals that over the RQ-Ni catalyst 18% of eAQ was converted to 2-ethyltetrahydroanthrahydroquinone (H_4eAQH_2) and 3% of eAQ was deteriorated [4]. It is noted that the oxidation rate of H_4eAQH_2 is sharply slowed down compared to that of eAQH_2, leading to lower efficiency in H_2O_2 production [5]. Besides, H_4eAQH_2 can be further hydrogenated to 2-ethyloctahydroanthrahydroquinone (H_8eAQH_2) which does not produce H_2O_2 [3]. Although the nanosized Ni–Cr–B catalyst shows 100% selectivity in eAQ hydrogenation to H_2eAQ [5], its low thermal stability and difficulty in separation from the reaction products impede its practical application. Moreover, the Cr additive in the Ni–Cr–B catalyst is enviromentally hazardous.

Here we report on a mesoporous molecular sieve SBA-15-supported amorphous nickel boride alloy catalyst (denoted as Ni–B/SBA-15) prepared by a novel reductant–impregnation method. This Ni–B/SBA-15 catalyst exhibits higher activity and stability than the nanosized amorphous Ni–Cr–B catalyst and can efficiently block the hydrogenation of the aromatic rings in eAQ. Even after a reaction time of 240 min, the amount of eAQ only dropped by 6%, while no degradation products were detected. Along with its enviromentally benign nature, this novel Ni–B/SBA-15 catalyst shows an attractive perspective for industrial application.

* Corresponding authors.
E-mail addresses: mhqiao@fudan.edu.cn (M. Qiao), heyonghe@fudan.edu.cn (H. He).

0021-9517/$ – see front matter
doi:10.1016/j.jcat.2003.07.007

2. Experimental and methods

2.1. Catalyst preparation

Pure silicate SBA-15 was synthesized according to the well-established method designed by Zhao et al. with triblock poly(ethylene oxide)-b-poly(propylene oxide)-b-poly(ethylene oxide) copolymer (Pluronic, $EO_{20}PO_{70}EO_{20}$, P_{123}) as the template [6]. Then it was crushed and sieved to obtain a particle size of 40–60 meshes.

Ni–B/SBA-15 catalyst was prepared by the following procedure. The SBA-15 (1.0 g, 40–60 meshes) was immersed into a 3.0 M potassium borohydride solution (13.74 mmol) at 293 K for 15 min. The excessive solution was decanted and a 0.42 M nickel chloride solution (3.41 mmol) was poured into the flask containing SBA-15 to start the reduction. The mixture was placed undisturbed at 293 K until no bubbles were generated. The resulting black solids were washed with distilled water to neutrality and then with ethanol three times to replace water. The catalyst was finally kept in ethanol for characterization and activity tests.

For comparison, the ultrafine Ni–Cr–B catalyst was prepared by mixing K_2CrO_4 salt in the nickel chloride aqueous solution before potassium borohydride reduction as previously reported [5].

2.2. Catalyst characterization

The X-ray diffraction (XRD) patterns were collected on a Bruker AXS D8 Advance X-ray diffractometer with Cu-K_α radiation. The BET surface area and the pore volume were determined by N_2 physical adsorption at 77 K on a Micromeritics TriStar 3000 adsorption apparatus. The bulk compositions of the as-prepared catalysts were detected by inductively coupled plasma (ICP) analysis. The crystallization process and the crystallization temperature were determined by differential scanning calorimetry (DSC, Perkin-Elmer DTA-7) analysis which was carried out under nitrogen atmosphere (99.9995%) with a heating rate of 10 $K\,s^{-1}$. The active surface area was measured by H_2 chemisorption, taking H/Ni(s) = 1 and a surface area of 6.5×10^{-20} m^2 per Ni atom [7]. Turnover frequency (TOF) was expressed as the number of H_2 molecules consumed per active surface nickel atom per second at the beginning of the reaction. The types of active sites existing on the catalyst were studied by temperature-programmed desorption of H_2 (H_2-TPD). The pore structure and selected-area electron diffraction (SAED) pattern of the catalyst were acquired by a transmission electron microscope (TEM, JEM2011), fitted with an energy dispersive X-ray emission analyzer (EDX). The surface composition and electronic state were detected by X-ray photoelectron spectroscopy (XPS, Perkin-Elmer PHI 5000C). All binding energy (BE) values were referenced to that of contaminant carbon (C 1s = 284.6 eV).

2.3. Reaction and analytical procedures

The activity test was carried out in a 220-ml stainless-steel autoclave with a magnetic stirrer. A mixture of trioctylphosphate and trimethylbenzene (volume ratio 3/7) was used as the solvent and the concentration of eAQ in the working solution was 50 $g\,l^{-1}$. The reaction conditions were as follows: 70 ml of working solution, 1.0 g of catalyst, reaction temperature of 323 K, H_2 pressure of 0.3 MPa, and a stirring rate of 1000 rpm to exclude diffusion effects. The reaction process was monitored by sampling the reaction mixture at intervals for O_2 oxidation. The H_2O_2 produced was extracted by distilled water and then titrated with $KMnO_4$. The percentage yield of H_2O_2 (X) is expressed as the ratio of the molar number of H_2O_2 to the initial molar number of eAQ in the reactor, i.e., $X = n^t_{H_2O_2}/n^0_{eAQ} \times 100\%$, which also represents the selectivity to H_2eAQ and H_4eAQH_2. The organic layer was further analyzed by HPLC (HP 1100) with an ultraviolet detector and the Zorbax column (ODS, 4.6 mm × 15 cm) to quantify eAQ and H_4eAQ.

3. Results and discussion

The nickel loading of the as-prepared catalyst is 9.84 wt% with a chemical composition of $Ni_{57.7}B_{42.3}$ (molar ratio) as determined by ICP analysis. The pore diameter of the catalyst calculated by the BJH method is 6.5 nm and the BET surface area is 367 $m^2\,g^{-1}$. The pore volume of the catalyst (0.482 $cm^3\,g^{-1}$) remarkably drops as compared to that of the original SBA-15 (1.233 $cm^3\,g^{-1}$), suggesting the incorporation of the nickel boride particles in the SBA-15 channels. TEM unambiguously confirmed this suggestion and further revealed that the nickel boride particles (the darker ones as verified by EDX) were uniformly dispersed in the SBA-15 channels (Fig. 1a). The average particle size of the Ni–B amorphous alloy in the Ni–B/SBA-15 catalyst is ∼6.5 nm. It is worth noting that on mesoporous MCM-41 or HMS molecular sieve-supported nickel boride catalysts prepared in the same way, the amorphous Ni–B alloy particles are mainly located outside the mesopores with scattered particle-size distributions ranging from 20 to 60 nm (Fig. 1b).

XRD patterns of original SBA-15 and Ni–B/SBA-15 catalysts verified the intact framework of SBA-15 in the catalyst. For the Ni–B/SBA-15 sample, besides the typical SBA-15 diffraction peaks, one broad peak centered at $2\theta = 45°$, characteristic of the amorphous nature of Ni–B [8] was observed, which was further confirmed by SAED, as only a diffractive halo was observed (inset in Fig. 1). DSC demonstrated the superior thermal stability of the as-prepared catalyst, as its crystallization temperature is 80 K higher than that of ultrafine Ni–Cr–B [5]. XPS spectra showed that in the Ni–B/SBA-15 catalyst Ni is predominantly in its elemental state [9]. However, the B1s-binding energy is ∼1.2 eV higher than that of pure amorphous B. This implies that boron donates electron to nickel in the Ni–

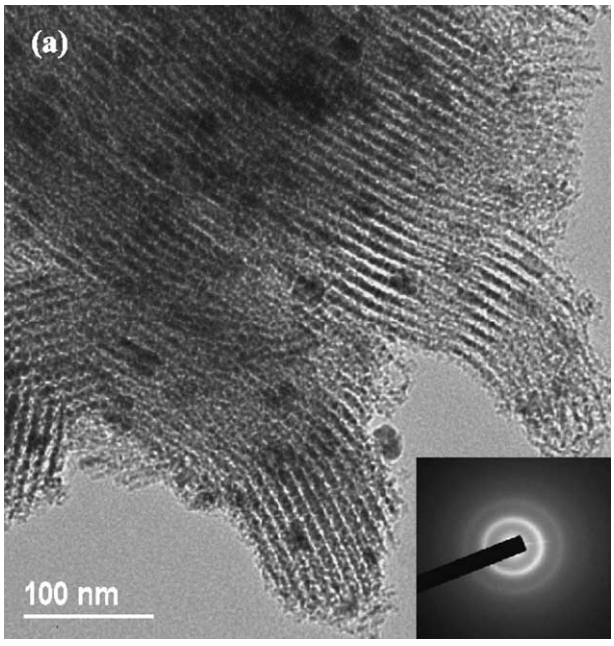

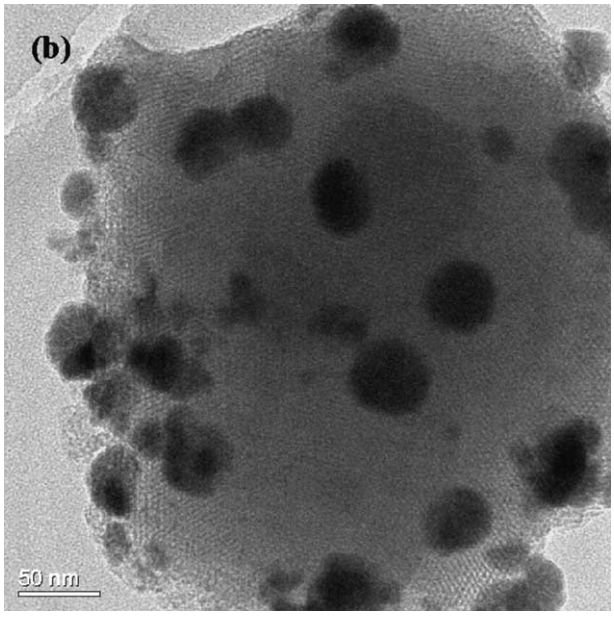

Fig. 1. TEM images of (a) Ni–B/SBA-15 (inset showing its SAED pattern) and (b) Ni–B/MCM-41 catalysts.

B/SBA-15 catalyst, resulting in electron-rich metallic Ni [9]. Moreover, the H_2-TPD profile of the catalyst exhibited only one peak at ~ 700 K, from which we infer the uniformity of the active sites on the catalyst.

Fig. 2 presents the percentage yield of H_2O_2 over the Ni–B/SBA-15 catalyst as a function of time. To get a deeper insight into the selectivity, the evolution of eAQ and H_4eAQ was also plotted as an inset. It should be stressed that eAQ virtually denotes the summation of unreacted eAQ and eAQ hydrogenated to H_2eAQ, while H_4eAQ is equal to H_4eAQH_2 in quantity, as illustrated by the reduction–oxidation cycle [4]. As Fig. 2 shows, the H_2O_2 yield over Ni–B/SBA-15

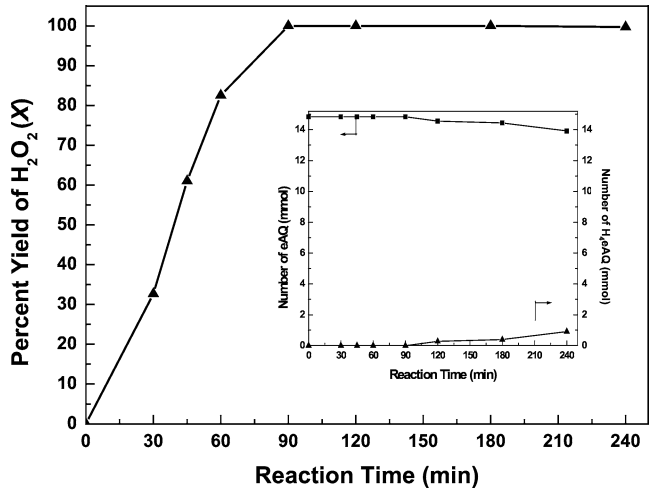

Fig. 2. The percentage yield of H_2O_2 (X). Inset is the evolution of eAQ and H_4eAQ over the Ni–B/SBA-15 catalyst as a function of reaction time (reaction conditions: [eAQ] $= 50$ g L^{-1}, $T = 323$ K, $P_{H_2} = 0.3$ MPa, $r_s = 1000$ rpm, $W_{cat} = 1.0$ g).

increased steeply up to $\sim 100\%$ in a reaction time of 90 min and then began to fall marginally. The TOF of the Ni–B/SBA-15 catalyst in this reaction is 0.12 s^{-1}, which is much larger than the value found for the ultrafine Ni–Cr–B catalyst (~ 0.03 s^{-1}), demonstrating the superior activity of the Ni–B/SBA-15 catalyst. HPLC analysis showed that the amount of eAQ remained constant and no H_4eAQ was detected within the first 90 min (inset in Fig. 2). Prolonged reaction time led to a decrease in the amount of eAQ and simultaneously an increase of H_4eAQ. Nevertheless, even after a reaction time of 240 min, the amount of eAQ only dropped by 6%, while no degradation products appeared. This clearly demonstrates the excellent selectivity of the Ni–B/SBA-15 catalyst. Moreover, the catalyst is highly stable, as confirmed by its invariable catalytic behavior in successive runs and virtually unchanged TEM feature of the used catalyst. In contrast, there was evidence for the lower thermal stability and significant leaching of the active component on the MCM-41 or HMS-supported Ni–B catalyst. Here the time for achieving the maximum H_2O_2 yield was prolonged to 180 min.

From the characterization and the activity test shown above, the superior activity and selectivity of Ni–B/SBA-15 in carbonyl group hydrogenation can be addressed as follows. First, due to the isotropic nature of the amorphous alloy [10], the active center on the present catalyst is expected to be more homogeneous, which is the prerequisite for the high selectivity. On the other hand, the coordinatively unsaturated structure of the amorphous alloy [10] makes it bind tightly with hydrogen, which is disadvantageous for the hydrogenation of the aromatic ring [11]. The H_2-TPD result is in support of our hypothesis. Second, owing to the unique electron state of the amorphous nickel boride alloy [12], the electrons are prone to transfer from the electron-rich nickel to the π^* antibonding orbitals of the carbonyl group, which induces a suitable adsorption configuration for the activation

and hydrogenation of the carbonyl groups, therefore promoting the selectivity in eAQ hydrogenation. Third, the unique pore structure of SBA-15 [6,13] may also contribute greatly to the superior performance of the Ni–B/SBA-15 catalyst. The large pore size of the SBA-15 mesoporous molecular sieve ($\sim$6.5 nm) makes it possible for the amorphous Ni–B alloys to be formed inside the SBA-15 channels as verified by the TEM image. Thus the aggregation of the nanosized particles can be readily impeded by the isolation of the channel walls. At the same time, the mesopores of SBA-15 are large enough for the diffusion and reaction of eAQ inside the SBA-15 channels. The pore size of MCM-41 or HMS (<3 nm) may be too small to incorporate the amorphous Ni–B particles, thus leading to inferior stability and less active sites accessible by the reactants.

4. Conclusions

Over the Ni–B/SBA-15 catalyst, the hydrogenation of the aromatic ring in eAQ is essentially suppressed, leading to a high yield of H_2O_2 and less consumption of eAQ. The unique characters of the amorphous alloy and the pore structure of the mesoporous SBA-15 molecular sieve are crucial for its excellent catalytic behavior.

Acknowledgments

This work was supported by the State Key Basic Research Development Program (G2000048009) and the National Science Foundation of China (20005310, 20073008, 20203004).

References

[1] C.S. Cronan, Chem. Eng. 6 (1959) 118.
[2] T. Ulmann, in: Encyclopedia of Industrial Chemistry, Vol. A3, VCH, Weinheim, 1989, p. 443.
[3] J.I. Kroschwitz, M. Howe-Grant, in: Kirk-Othmer Encyclopedia of Chemical Technology, Vol. 13, 4th ed., Wiley, New York, 1995, p. 961.
[4] B. Liu, M.H. Qiao, J.F. Deng, K.N. Fan, X.X. Zhang, B.N. Zong, J. Catal. 204 (2001) 512.
[5] B. Liu, M.H. Qiao, J.Q. Wang, K.N. Fan, Chem. Commun. (2002) 1236;
H.X. Li, W.J. Wang, H. Li, J.F. Deng, J. Catal. 194 (2000) 211.
[6] D.Y. Zhao, J.L. Feng, Q.S. Huo, N. Melosh, G.H. Fredrickson, B.F. Chmelka, G.D. Stucky, Science 279 (1998) 548.
[7] C.H. Bartholomew, R.B. Pannell, J. Catal. 65 (1980) 390.
[8] J. Wonterghem, S. Mørup, S.W. Charles, S. Wells, Nature 322 (1986) 622.
[9] Handbook of X-Ray Photoelectron Spectroscopy, Perkin–Elmer Corporation, 1992.
[10] A. Molnar, G.V. Smith, M. Bartok, Adv. Catal. 36 (1989) 329.
[11] S.D. Mikhailenko, A.B. Fasman, N.A. Maksimova, E.V. Leongard, Appl. Catal. 12 (1984) 141.
[12] J.F. Deng, J. Yang, S.S. Sheng, H.Y. Chen, X.G. Xing, J. Catal. 150 (1994) 434.
[13] D.Y. Zhao, Q.S. Huo, J.L. Feng, B.F. Chmelka, G.D. Stucky, J. Am. Chem. Soc. 120 (1998) 6024.